11^{th} International Conference on Fracture Mechanics of Concrete and Concrete Structures
FraMCoS-11
J. M. Chandra Kishen, A. Ramaswamy, S. Ray and R. Vidyasagar (Eds)
https://doi.org/10.21012/FC11.092385

MULTI-PHYSICS SIMULATION OF CORROSION-INDUCED CRACKING OF CONCRETE BY MEANS OF A MESOSCOPIC MODELING APPROACH

Yue Li[†‡*], Xin Ruan[†], Herbert A. Mang[†‡], and Bernhard L.A. Pichler[‡]

[†]Department of Bridge Engineering, Tongji University
Shanghai, China
e-mail: yueli@tongji.edu.cn

[‡]Institute for Mechanics of Materials and Structures, TU Wien (Vienna University of Technology)
Vienna, Austria, European Union
e-mail: yue.li@tuwien.ac.at

Key words: Concrete, Corrosion-induced cracking, Mesoscopic modeling, Multiphysics simulation

Abstract. Corrosion-induced cracking is a deterioration problem. It endangers the durability of concrete infrastructure. It is a multi-physics process which includes the transport of chemically aggressive ions from the surface of a reinforced concrete structure, through the mesostructure of concrete, to the steel rebars. Corrosion results in a volume expansion of steel. The corresponding development of tensile stresses of the concrete leads to cracking. This is particularly the case in the cover region between the rebars and the surface of the structure. Many experiments have provided insight into the governing physicochemical mechanisms. Together with recent progress in the area of material modeling techniques and advanced computation technologies, several promising approaches for the numerical simulation of corrosion-induced cracking have been developed. In order to further extend this development, it is indispensable to model concrete as a heterogeneous material containing aggregates with realistic shapes and distributions. It is necessary to treat the rust-formation as non-uniformly distributed around the perimeter of the steel rebars. These items provided the motivation for the development of a multi-physics model for corrosion-induced cracking of concrete, which resolves the mesostructure of reinforced concrete in a two-dimensional fashion, by explicitly accounting for steel, aggregates, interfacial transitions zones (ITZs), and the mortar matrix. Results obtained from numerical modeling are compared with experimental data taken from the open literature. In order to demonstrate the potential and the limitations of the approach, the study also contains a sensitivity analysis with the size of finite elements as the parameter. It is recommended to use an element size of 4.0 mm. This is a reasonable compromise between accuracy and numerical efficiency.

1 INTRODUCTION

Corrosion-induced cracking is one of the most commonly encountered durability problems of reinforced concrete structures. Almost all reinforced concrete structures in operation are affected by this multi-physics problem, which jeopardizes their serviceability and safety in the long term.

This motivated leading experimenters to perform tests both in situ and in the laboratory, in order to gain quantitative insight into the governing physicochemical mechanisms and their interaction. Andrade et al. [1] used electric current to accelerate the corrosion of steel rebars embedded in cuboidal concrete specimens. They studied crack propagation as a function of the rate of corrosion and the depth of the

concrete cover. Gao et al. [2] investigated the randomness of chloride profiles resulting from the exposure of reinforced concrete specimens to natural and simulated tidal environments, respectively. Du et al. [3] studied similarities and differences between accelerated corrosion testing in the laboratory and in situ marine exposure. Michel et al. [4] monitored the corrosion of steel reinforcements for five years, performing in situ tests in the splash zone and submerged in sea water, respectively. These experimental campaigns revealed quantitative relations between corrosion rates and the speed at which crack widths evolve. The collected data are very valuable for the development and the validation of models, aimed at providing long-term predictions of the deterioration of reinforced concrete structures exposed to aggressive environments.

Several numerical models were published in the past decade, see e.g. [5–8]. Accounting for specific geometric properties of the simulated structures and their exposure conditions, these models simulate the transport of ions, the corrosion reaction, and concrete cracking. From the cited studies, it is concluded that the heterogeneous nature of the mesostructure of concrete has an important influence on the diffusive transport of ions into reinforced concrete structures and, therefore, indirectly on cracking of the concrete cover. This provides the motivation to introduce methods for material modeling which resolve the mesostructure of concrete and account for important properties of the aggregates, including distribution of their particle size, their random shapes, and their disordered arrangement inside the volume of concrete [9]. Several models have been proposed to describe the corrosion reaction and the corresponding expansion of the volume of steel, resulting from its oxidation under different environmental exposure conditions [10]. As for the simulation of cracking of concrete, advanced methods, among them the extended finite element method and phase field methods, are frequently used [11, 12]. Understanding of the governing physicochemical processes, advanced theoretical models, and powerful numerical tools render the simulation of the chain of processes, ranging from ion transport to concrete cracking, possible. This is the focus of the present contribution.

The paper is organized as follows: Section 2 deals with the presentation of the methods used for simulation of accelerated corrosion-induced cracking under explicit consideration of the heterogeneous mesostructure of concrete. Section 3 is devoted to the comparison of results obtained from modeling with experimental data taken from the open literature. Section 4 refers to the influence of the size of the finite elements on the results of the numerical simulations. Section 5 contains the conclusions drawn from the results of the presented study.

2 SIMULATION METHODS

2.1 Two-dimensional representation of the heterogeneous mesostructure of concrete

Mesoscopic modeling of concrete accounts for the complex geometric properties resulting from the disordered arrangement of aggregate particles of different sizes and shapes. In the following, a two-dimensional representation of the heterogeneous mesostructure of concrete will be described.

The probability distribution of the size of aggregate particles was investigated in several studies, see e.g. [13]. The characteristic size of an aggregate particle, D, is usually set equal to the diameter of a round particle occupying the same area. Walraven et al. [14] developed the following cumulative distribution function (CDF) for the description of characteristic sizes of aggregates, which reproduces the grading curve proposed by Fuller:

$$\begin{aligned}\mathrm{CDF}(D) = 1.065\,\eta^{0.5} - 0.053\,\eta^{4.0} - 0.012\,\eta^{6.0} \\ - 0.0045\,\eta^{8.0} + 0.0025\,\eta^{10.0}\,,\end{aligned} \tag{1}$$

with

$$\eta = \frac{D}{D_{max}}\,, \tag{2}$$

where D_{max} denotes the largest characteristic

size of the aggregate particles.

The contours of the aggregate particles are modeled by means of polygons. The shape of each polygon is described by an aspect ratio, Υ, which is equal to the length ratio of the longest and the shortest axis. The probability distribution function (PDF) of Υ was back-analyzed from images showing cross-sections of real concrete mesostructure [15]. This PDF follows the General Extreme Value distribution function:

$$\mathrm{PDF}(\Upsilon) = \exp\left[-\left(1+\xi\frac{\Upsilon-\mu}{\sigma}\right)^{-\frac{1}{\xi}}\right], \quad (3)$$

with the side condition

$$1+\xi\,\frac{\Upsilon-\mu}{\sigma} > 0\,, \quad (4)$$

where μ, σ, and ξ denote a local, scale, and shape parameter, respectively. Herein, the following recommended numerical values are used [15]:

$$\mu = 1.612\,, \quad (5)$$
$$\sigma = 0.457\,, \quad (6)$$
$$\xi = 0.278\,. \quad (7)$$

The mesostructure of concrete is modeled in a step-wise fashion. At first, a random population of aggregates is produced, following the CDF according to Eqs. (1) and (2) and the PDF according to Eqs. (3)–(7). For every single aggregate, a basic polygon is generated by connecting random vertices on the edge of a circle. This is followed by scaling and stretching of the polygon in order to obtain the required size and aspect ratio of the specific aggregate. Finally, all generated polygons are randomly rotated and placed into a simulation area, whereby the overlap of neighboring particles is avoided.

2.2 Corrosion simulation

The corrosion reaction on the steel-concrete interface is driven by the applied electric current. Based on available literature, e.g. [16], concrete is treated as the conductor obeying Ohm's law. The spatial distribution of the electric potential, ϕ, fulfills the following partial differential equation:

$$\nabla\left(\frac{1}{\rho}\,\nabla\phi\right) = 0\,, \quad (8)$$

where ∇ denotes the Laplace operator, and ρ stands for the effective resistivity with the physical unit $\Omega\,\mathrm{m}$, obtained from experiments. The flux of the electric current, $\boldsymbol{i}$, is proportional to the gradient of the electric potential:

$$\boldsymbol{i} = -\frac{1}{\rho}\nabla\phi\,. \quad (9)$$

The corrosion rate on the surface of the steel rebars is proportional to the local current density, such that the depth of penetration of the corrosion front into the rebar, u_c, is proportional to the time-integral of the current density:

$$u_c(t) = \frac{A_s\int_0^t \boldsymbol{i}\cdot\boldsymbol{n}\,\mathrm{d}t}{\rho_s\,F\,z_{Fe}}\,. \quad (10)$$

In Eq. (10), $55.85\,\mathrm{g\,mol^{-1}}$ is the value of the atomic weight of iron, A_s; t denotes the time variable; $\boldsymbol{n}$ stands for the local normal unit vector to the reinforcement surface; $7.8\,\mathrm{g\,mm^{-3}}$ is the value of the mass density of iron, ρ_s; $F = 9.6485\times10^4\,\mathrm{C/mol}$ is Faraday's constant, and $z_{Fe} = 2$ is the valency of the anodic reaction. The volume of the produced rust is proportional to the volume of corroded iron. Disregarding, for the sake of simplicity, both the compression-induced compaction of rust and its transport by means of flow, the local expansion, u_r, of the rebar is proportional to the local depth of penetration of the corrosion front into the rebar, u_c, i.e.

$$u_r = (\alpha_r - 1)\,u_c\,, \quad (11)$$

where α_r denotes the volume ratio of rust and corroded iron. Following Suda et al. [17], α_e is set equal to 2.96.

2.3 Simulation of cracking of concrete

Cracking of concrete is simulated in the framework of continuum damage mechanics. A

scalar damage variable, d, is established to describe the deterioration of the elastic stiffness

$$\boldsymbol{\sigma} = (1-d)\boldsymbol{C} : \boldsymbol{\varepsilon}\,, \tag{12}$$

where $\boldsymbol{\sigma}$ denotes Cauchy's stress tensor, $\boldsymbol{C}$ stands for the fourth-order elasticity tensor describing the initial (undamaged) elastic stiffness of the material, and $\boldsymbol{\varepsilon}$ denotes the linearized strain tensor: The damage variable d ranges from zero to one: $d = 0$ and $d = 1$ indicate the intact initial state and the complete loss of stiffness, respectively.

Adopting exponential strain softening, the damage variable d obeys the following evolution law

$$d(\kappa) = \begin{cases} 0\,, & \kappa \leq \varepsilon_{cr}\,, \\ 1 - \dfrac{\varepsilon_{cr}}{\kappa}\exp\left(\dfrac{\kappa-\varepsilon_{cr}}{\varepsilon_f-\varepsilon_{cr}}\right)\,, & \kappa > \varepsilon_{cr} \end{cases}\,, \tag{13}$$

where κ denotes a state variable, equal to the maximum nonlocal equivalent strain $\overline{\varepsilon_{eq}}$ experienced by the material, ε_f stands for a strain-like parameter, relevant to the description of the strain softening regime, and ε_{cr} denotes the critical elastic strain for the onset of damage under uniaxial tension. It is calculated from the tensile strength σ_{ts} and the modulus of elasticity E of intact (undamaged) concrete:

$$\varepsilon_{cr} = \frac{\sigma_{ts}}{E}\,. \tag{14}$$

The nonlocal equivalent strain $\overline{\varepsilon_{eq}}$ and the parameter ε_f will be explained in the following.

The crack-band method is used for regularization of the strain-softening behavior. The *nonlocal* equivalent strain

$$\overline{\varepsilon_{eq}} = \int_\Omega \phi_r(\boldsymbol{x},\boldsymbol{\xi})\,\varepsilon_{eq}(\boldsymbol{\xi})\,\mathrm{d}\boldsymbol{\xi}\,, \tag{15}$$

is introduced [18]. ε_{eq} is the local equivalent strain. It is calculated from the positive (= tensile) principal strain components [19]:

$$\varepsilon_{eq} = \sqrt{\langle\varepsilon_1\rangle^2 + \langle\varepsilon_2\rangle^2}\,, \tag{16}$$

where ε_1 and ε_2 are the principal strains; the angled brackets denote the Macaulay operator, defined as $\langle\varepsilon_i\rangle = \big(|\varepsilon_i| + \varepsilon_i\big)/2$. $\phi_r(\boldsymbol{x},\boldsymbol{\xi})$ denotes the normalized nonlocal weighting function, describing the contribution of the local equivalent strain at location $\boldsymbol{\xi}$ to the nonlocal equivalent strain at location $\boldsymbol{x}$:

$$\phi_r(\boldsymbol{x},\boldsymbol{\xi}) = \frac{\phi_{r,0}(\boldsymbol{x},\boldsymbol{\xi})}{\int_\Omega \phi_{r,0}(\boldsymbol{x},\boldsymbol{\xi})\,\mathrm{d}\boldsymbol{\xi}}\,. \tag{17}$$

In Eq. (17), $\phi_{r,0}$ is a bell-shaped function that decreases with increasing distance $r = \|\boldsymbol{x}-\boldsymbol{\xi}\|$:

$$\phi_{r,0}(\boldsymbol{x},\boldsymbol{\xi}) = \left\langle 1 - \frac{r^2}{l_c^2}\right\rangle^2\,, \tag{18}$$

where l_c is a characteristic length related to the size of the used finite elements. The Macaulay operator in Eq. (18) ensures that $\phi_r(\boldsymbol{x},\boldsymbol{\xi})$ is equal to 0 in regions where r is larger than l_c. Thus, l_c denotes the boundary of the integration domain Ω in Eq. (15), serving as a localization limiter leading to mesh insensitivity.

Following Rots et al. [20], the crack width w is introduced as

$$w = l_c\,\varepsilon_{cw}\,, \tag{19}$$

where

$$\varepsilon_{cw} = \overline{\varepsilon_{eq}} - \frac{\sigma_1}{E}\,. \tag{20}$$

In Eq. (20), σ_1 stands for the larger principal stress ($\sigma_1 \geq \sigma_2$).

In the crack-band method, the parameter ε_f of the exponential strain softening in Eq. (13), is determined by the energy dissipation during the fracture process. Based on the fracture energy G_f (the energy dissipated per unit area crack), ε_f reads as

$$\varepsilon_f = \frac{G_f}{\sigma_{ts}\,l_c} + \frac{\varepsilon_{cr}}{2}\,. \tag{21}$$

3 RESULTS AND MODEL VALIDATION

3.1 Simulation set-up

To assess the accuracy of the proposed numerical method, it is checked to which extent it is possible to reproduce the test results reported by Andrade et al. [1]. The analyzed experiment

refers to a cuboidal concrete specimen with dimensions $150\,\mathrm{mm} \times 150\,\mathrm{mm} \times 380\,\mathrm{mm}$. It contains one $16\,\mathrm{mm}$-diameter ordinary corrugated steel rebar which is placed in the specimen parallel to its longest axis. The concrete has a tensile strength amounting to $3.55\,\mathrm{MPa}$ [1]. In order to accelerate corrosion, an electrical current is applied to the rebar. The average current density on the surface of the rebar is equal to $100\,\mu\mathrm{A\,cm^{-2}}$ [1]. The accelerated corrosion test runs for 34 days. The numerical simulations refer to a two-dimensional cross-section through the specimen, normal to the axis of the rebar, see Fig. 1(a). The computation of the corrosion reaction and crack propagation is performed by means of the COMSOL Multiphysics software. The following simulation results will be compared to the experimental data: (i) crack patterns and (ii) crack opening widths, observed and measured during testing, see [1].

Five different two-dimensional mesostructural representations of concrete were analyzed. They are referred to as Model-1 to Model-5. All of them have a size of $150\,\mathrm{mm} \times 150\,\mathrm{mm}$, representing the cross-section of the three-dimensional specimens described above. The embedded rebars are considered in the model. For each one of the five different models, a unique concrete mesostructure is randomly generated in the quarter of the cross-section around the rebar, see the top-right quarter of Fig. 1(a). The aggregate particles are represented as polygons, with sizes ranging from $0.5\,\mathrm{mm}$ to $25.0\,\mathrm{mm}$. In the remaining other three quarters of the model, concrete is introduced as an equivalent homogeneous material. The simulation domain is discretized by means of free triangular meshing. The characteristic sizes of every triangular finite element, d_e, is proportional to the square-root of its area, a_e. Herein, the following definition is used:

$$d_e = \sqrt{2a_e}\,. \tag{22}$$

Notably, d_e is equal to the length of the legs in the case of an isosceles right triangle. Herein, the characteristic size of the finite elements is smaller than $4\,\mathrm{mm}$. Taking Model-1 as an example, the geometrical model is discretized with 7,270 triangular finite elements. The mesh consists of 3,687 nodes. Different elements refer to the aggregates, the cement mortar, and the homogenized concrete, see Table 1 for the material properties of the three different solid phases. The thickness of the ITZs amounts to 20 - $50\,\mu\mathrm{m}$. This is much smaller than the size of the aggregates. Therefore, the ITZs are represented using edge elements, introduced between the aggregates and the cement mortar matrix. The electrical potential, the deformation, and the stresses are allowed to be discontinuous across the ITZ. Corresponding jumps of the physical quantities are calculated based on the properties and the thickness of the ITZ, see [21] for the details, and Table 1 for the material properties assigned to the ITZs.

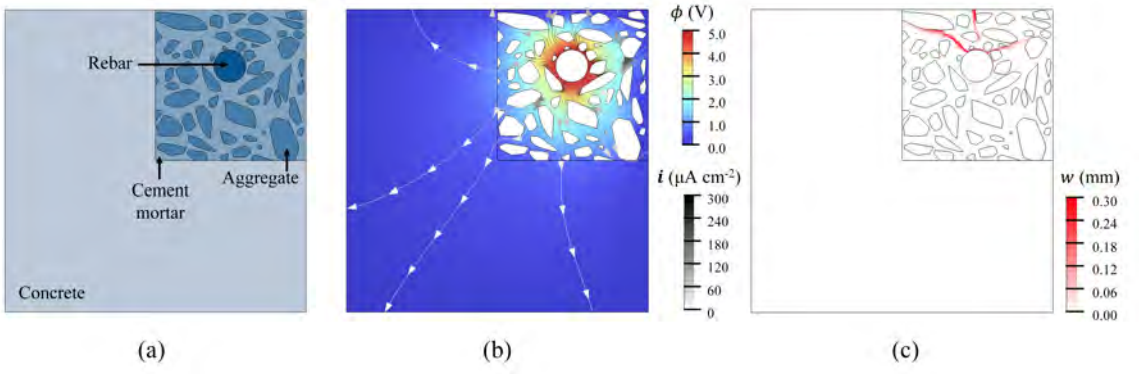

Figure 1: Simulation results of model 1: (a) geometric model, (b) distribution of the electrical potential, see the colors, and illustration of current flux, see the gray curves with arrows, and (c) distribution of cracks and corresponding crack opening widths.

Table 1: Mechanical properties of concrete, aggregates, mortar, and ITZ.

Properties	Concrete	Aggregates	Mortar	ITZ
Young's modulus (GPa)	33.0	70.0	25.0	15.0
Poisson's ratio	0.2	0.2	0.2	0.2
Failure strength (MPa)	3.8	8.0	4.0	2.5
Fracture energy $(\mathrm{N\,m})$	95.0	-	60.0	20.0

The average current density $100\,\mu\mathrm{A\,cm^{-2}}$ is introduced into the numerical model by applying a total current of $502.65\,\mu\mathrm{A\,cm^{-1}}$ to the rebar, noting that the circumference of the rebar amounts to $50.27\,\mathrm{mm}$. At the outer edges of the simulation domain, the electrical potential is set equal to zero (= boundary condition). The spatial distributions of the electric potential ϕ and of the current flux $\boldsymbol{i}$ are computed inside the cement mortar phase. The corrosion reaction and the depth of penetration of the corrosion front into the rebar are calculated based on Eq. (10). Notably, the electrical current density and the depth of corrosion are non-uniformly distributed across the cross-section of the rebar.

As regards the simulation of concrete cracking, the non-uniform distribution of u_r around the concrete-iron interface is calculated based on Eq. (11) and imposed on the boundary of the concrete phase. The bottom edge of the model is prevented from undergoing rigid body displacements. In the plane strain simulations, crack propagation processes are calculated in an incremental-iterative manner. 340 time steps, with a duration of 0.1 days, are used to simulate a process extending over 34 days. The crack widths at the specimen's surfaces are quantified for every time-instant of the simulation.

3.2 Comparison of simulation results with experimental measurements

For each one of the five models, the crack widths are quantified at the top edge and the right lateral edge of the simulation domain. These numerical results are compared with test results [1], see Fig. 2.

Because rebar corrosion and rust expansion takes time, the first crack reaches the top surface of the simulated specimen only during the 5^{th} day after applying the electrical current. The crack width increases monotonously to about $0.15\,\mathrm{mm}$ during the following days.

The mesostructure of concrete around the rebars has a significant influence on the evolution of the crack widths, see the differences in the results obtained by the five different models, illustrated in Fig. 2 by five colored solid lines and five colored dotted lines, respectively. The largest crack width is obtained for the fourth model. It exceeds $0.15\,\mathrm{mm}$ during the 13^{th} day, see the green solid line in Fig. 2. The smallest crack width is obtained for the second model. It reaches $0.02\,\mathrm{mm}$ only at the end of the 34^{th} day, see the blue dotted line in Fig. 2.

As regards the evolution of the simulated crack widths, the basic trends and orders of magnitudes are similar to the test results, as follows from a comparison of the colored lines with the black lines in Fig. 2. Given that the representation of the mesostructure of concrete has such a significant influence on the simulated cracking process, better agreement between simulation and experimental results cannot be expected.

4 DISCUSSION

4.1 Non-uniform rust formation around the rebar

The simulation results allow for investigating the detailed distribution of the corrosion products around the circumference of the rebar and the influence of the heterogeneity of concrete on this distribution. As for the first model, the mesostructure is shown in the top-right quarter of Fig. 1 (a). The electric potential decreases along the current flow lines from the

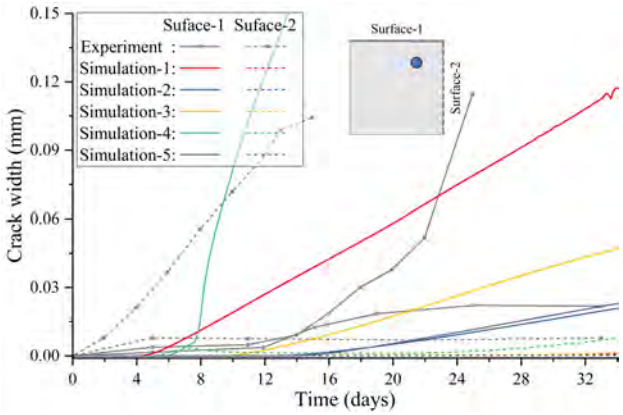

Figure 2: Validation of the numerical model: comparison of simulated and measured crack widths at the surface of the simulated and tested specimens; experimental results were taken from [1].

rebar surface to the specimen surface. The flow lines are clearly influenced by the mesostructure of concrete. The gradient of the electric potential and the current flux are the larger, the narrower the channels are between neighboring aggregate particles. This effect is responsible for the non-uniform distribution of corrosion products around the surface of the rebar surface, see Fig. 1(b).

4.2 Crack propagation through the mesostructure of concrete

The simulated cracks propagate from the rebar surface, mostly along the ITZs, to the surface of the specimen, see Fig. 1(c). The reason why ITZs are preferred crack paths is their smaller strength compared to the one of the cement mortar matrix and of the aggregates, see Table 1. The simulation results suggest that (i) there are several cracks inside the volume of the simulated specimens and (ii) not all of them reach the surface. The maximum crack width inside the volume of the specimen reaches some $0.30\,\mathrm{mm}$. This is almost twice as large as the largest crack width, visible at the surface of the specimen.

4.3 Comparison of numerical results obtained with five different representations of the mesostructure of concrete

Even though *the same* current was applied to the rebar in the five simulations, the obtained electric potentials at the surfaces of the rebar are different. In addition, after *the same* exposure to accelerated corrosion, the crack distributions and crack widths are remarkably different, see Fig. 3. This suggest to relate these differences to the differences regarding the specific aggregate arrangement. There are large aggregate particles quite close to the rebar surfaces in models 1, 3, and 4. In their vicinity, relatively high electric potentials are obtained at the rebar surface. In these models, the largest crack widths are obtained. The electrically insulating aggregate particles, positioned close to the rebar, seem to increase the electrical resistivity of the concrete cover. The ITZs, covering the aggregates close to the rebar, become the locus minoris resistentiae for local cracking.

4.4 Convergence analysis regarding the element size

Model-1 was analyzed four times, see Fig. 4. The same mesostructure of concrete was discretized with triangular finite elements with a maximum size of 2.0 mm, 4.0 mm, 8.0 mm and 16.0 mm, respectively. This was done in order to demonstrate the influence of the characteristic size of the finite elements on the properties of the simulated cracks.

Quantitatively, the cracks obtained with characteristic element sizes of 2.0 mm and 4.0 mm, respectively, are quite similar, see the leftmost two sketches in Fig. 4 showing crack patterns. As for the quantitative comparison, the crack widths were analyzed at the top sur-

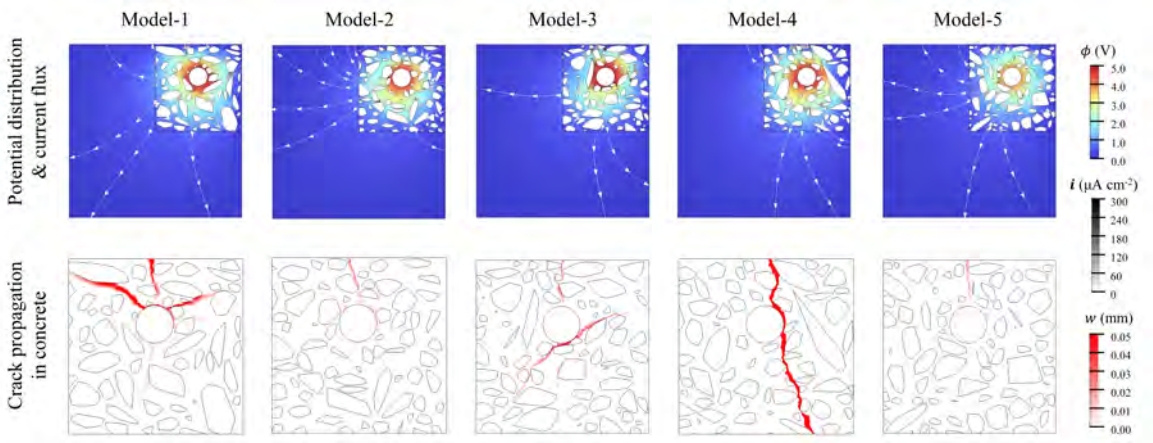

Figure 3: Simulation results of five models, including the potential distribution and the distributions of the current flux and crack width.

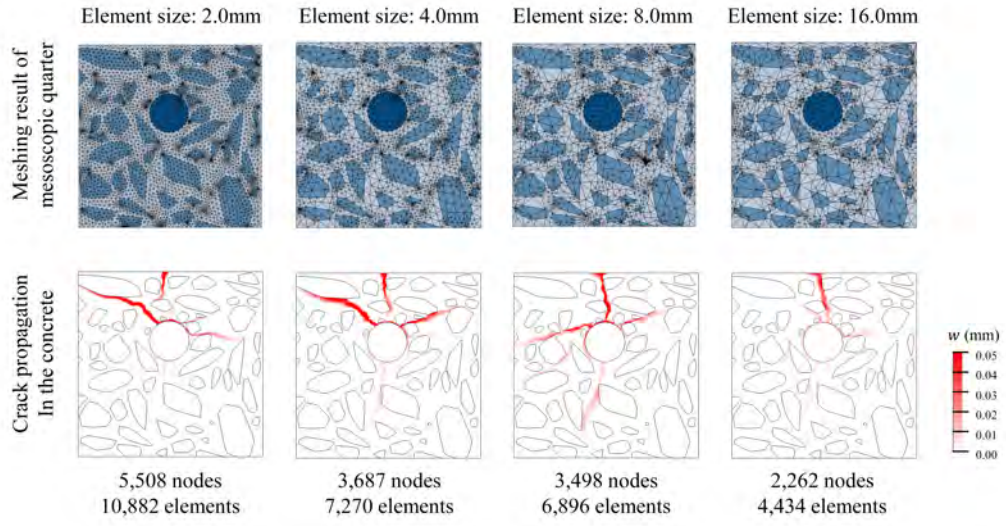

Figure 4: Analysis of Model-1, discretized by means of 10,882, 7,270, 6,896, and 4,434 triangular finite elements, respectively, with a maximum element size of 2.0mm, 4.0mm, 8.0mm and 16.0mm.

face. They are quite similar, as follows from comparing simulations with element sizes of 2.0 mm and 4.0 mm. The crack widths in the other two simulations are smaller, see Fig. 5.

The described qualitative and quantitative similarities and differences indicate that characteristic element sizes of 2.0 mm and 4 mm are sufficient for obtaining suitably converged numerical solutions. Considering that a larger element size reduces the number of elements and the associated computation efforts, a characersitic element size of 4.0 mm is recommended for resource-efficient two-dimensional simulations of corrosion-induced cracking in reinforced concrete structures.

5 CONCLUSIONS

From the results of the presented study, the following conclusions are drawn:

- Different random representations of the mesostructure of concrete lead to significantly different results when it comes to two-dimensional simulations of accelerated rebar corrosion and related concrete cracking of reinforced concrete specimens. This underlines that corrosion-induced damage of reinforced concrete structures requires many simulations with different representations of the mesostructure, followed by a statistical analysis of the simulation results.
- The heterogeneous nature of the mesostruc-

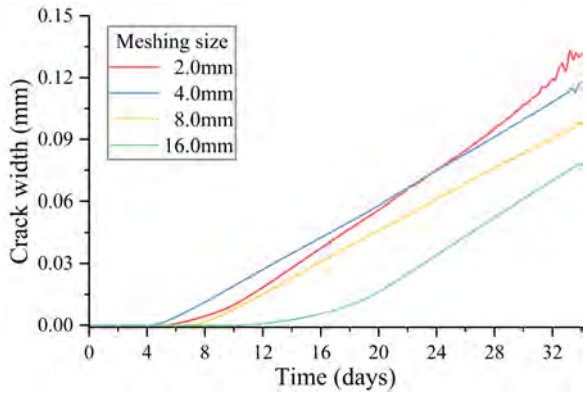

Figure 5: Comparison of crack widths on the concrete surface, obtained from simulations with different element sizes.

ture of concrete results in non-uniform rust formation around the perimeter of the rebars. The penetration depth of corrosion into the rebar is particularly large in regions where two aggregates are close both to each other and to the rebar, because the electrical current is particularly large inside the narrow mortar channel between the two neighboring aggregates.

• A convergence analysis regarding the discretization effort has shown that a maximum element size amounting to 4 mm is recommended for two-dimensional simulations of corrosion-induced cracking in reinforced concrete structures.

6 ACKNOWLEDGEMENT

Support from the China Scholarship Council (Grant number 202206260161) and the China Association for Science and Technology Outstanding Chinese and Foreign Youth Exchange Program (Grant number 0200151002) is gratefully acknowledged. Opinions and conclusions presented in this article are those of the authors and do not necessarily reflect the views of the sponsoring organizations.

REFERENCES

[1] C Andrade, C Alonso, and FJ Molina. Cover cracking as a function of bar corrosion: Part i-experimental test. *Materials and Structures*, 26:453–464, 1993.

[2] Yanhong Gao, Yingying Zheng, Junzhi Zhang, Jiandong Wang, Xiaoyun Zhou, and Yurong Zhang. Randomness of critical chloride concentration of reinforcement corrosion in reinforced concrete flexural members in a tidal environment. *Ocean Engineering*, 172:330–341, 2019.

[3] Fengyin Du, Zuquan Jin, Wei She, Chuansheng Xiong, Guangyan Feng, and Junfeng Fan. Chloride ions migration and induced reinforcement corrosion in concrete with cracks: a comparative study of current acceleration and natural marine exposure. *Construction and Building Materials*, 263:120099, 2020.

[4] Alexander Michel, Henrik E Sørensen, and Mette Rica Geiker. 5 years of in situ reinforcement corrosion monitoring in the splash and submerged zone of a cracked concrete element. *Construction and Building Materials*, 285:122923, 2021.

[5] Xiuli Du, Liu Jin, and Renbo Zhang. Modeling the cracking of cover concrete due to non-uniform corrosion of reinforcement. *Corrosion Science*, 89:189–202, 2014.

[6] Inamullah Khan, Raoul François, and Arnaud Castel. Prediction of reinforcement corrosion using corrosion induced cracks width in corroded reinforced concrete beams. *Cement and Concrete Research*, 56:84–96, 2014.

[7] Yuxi Zhao, Jianfeng Dong, Yingyao Wu, and Weiliang Jin. Corrosion-induced concrete cracking model considering corrosion product-filled paste at the concrete/steel interface. *Construction and Building Materials*, 116:273–280, 2016.

[8] Xun Xi, Shangtong Yang, and Chun-Qing Li. A non-uniform corrosion model and meso-scale fracture modelling of concrete. *Cement and Concrete Research*, 108:87–102, 2018.

[9] Branko Šavija, Mladena Luković, José Pacheco, and Erik Schlangen. Cracking of the concrete cover due to reinforcement corrosion: A two-dimensional lattice model study. *Construction and Building Materials*, 44:626–638, 2013.

[10] Bo Sun, Rucheng Xiao, Weidong Ruan, and Pengbo Wang. Corrosion-induced cracking fragility of rc bridge with improved concrete carbonation and steel reinforcement corrosion models. *Engineering Structures*, 208:110313, 2020.

[11] Shuo Yu and Hao Jin. Modeling of the corrosion-induced crack in concrete contained transverse crack subject to chloride ion penetration. *Construction and Building Materials*, 258:119645, 2020.

[12] Evžen Korec, Milan Jirásek, Hong S Wong, and Emilio Martínez-Pañeda. A phase-field chemo-mechanical model for corrosion-induced cracking in reinforced concrete. *Construction and Building Materials*, 393:131964, 2023.

[13] Tiejun Liu, Shanshan Qin, Dujian Zou, Wen Song, and Jun Teng. Mesoscopic modeling method of concrete based on statistical analysis of ct images. *Construction and Building Materials*, 192:429–441, 2018.

[14] JC Walraven. Aggregate interlock: a theoretical and experimental analysis [PhD thesis]. *The Netherlands: Delft University of Technology*, 1980.

[15] Xin Ruan, Yue Li, Zeren Jin, Zichao Pan, and Zhiyi Yin. Modeling method of concrete material at mesoscale with refined aggregate shapes based on image recognition. *Construction and Building Materials*, 204:562–575, 2019.

[16] SC Kranc and Alberto A Sagüés. Detailed modeling of corrosion macrocells on steel reinforcing in concrete. *Corrosion Science*, 43(7):1355–1372, 2001.

[17] Kumiko Suda, Sudhir Misra, and Kenichi Motohashi. Corrosion products of reinforcing bars embedded in concrete. *Corrosion Science*, 35(5-8):1543–1549, 1993.

[18] Milan Jirasek. Nonlocal models for damage and fracture: comparison of approaches. *International Journal of Solids and Structures*, 35(31-32):4133–4145, 1998.

[19] Jacky Mazars and Gilles Pijaudier-Cabot. Continuum damage theory—application to concrete. *Journal of Engineering Mechanics*, 115(2):345–365, 1989.

[20] P Nauta and GMA Kuster. Smeared crack approach and fracture localization in concrete. *HERON, 30 (1), 1985*, 1985.

[21] COMSOL. *Structural Mechanics Module User's Guide*. COMSOL, 1 edition, 12 2022.